Nuclear Engineering and Design 351 (2019) 87–93

Contents lists available at ScienceDirect

Nuclear Engineering and Design

journal homepage: www.elsevier.com/locate/nucengdes

Material, structural and modelling aspects of alkali aggregate reaction in concrete

Anca C. Ferche[a], Bishnu Gautam[b], Farhad Habibi[a], Daman K. Panesar[c,*], Shamim A. Sheikh[c], Frank J. Vecchio[c], Nebojsa Orbovic[d]

[a] Doctoral Candidate, Department of Civil and Mineral Engineering, University of Toronto, 35 St. George St., Toronto, ON M5S 1A4, Canada
[b] Member of a Province Planning Commission, Nepal and Former Doctoral Candidate, University of Toronto, Canada
[c] Department of Civil and Mineral Engineering, University of Toronto, 35 St. George St., Toronto, ON M5S 1A4, Canada
[d] Technical Specialist, Canadian Nuclear Safety Commission, Ottawa, ON, Canada

ARTICLE INFO

Keywords:
Alkali aggregate reaction
Expansion
Concrete
Multi-axial stresses
Shear wall
Modeling

ABSTRACT

Concrete nuclear structures have been identified as suffering from alkali aggregate reaction (AAR) in both Canada and the United States. Although much research effort has been directed toward understanding its effect on reinforced concrete structures, unresolved issues still remain. Among them are the effect of multiaxial stress states, commonly developed in nuclear structures, on the response of AAR-affected concrete; also of concern is the possible invalidity of conventional methods of analysis for structural assessment due to the induced anisotropy in the mechanical properties of concrete. The Canadian Nuclear Safety Commission initiated and funded an extensive study aimed to reveal the implications of concrete deterioration due to AAR on structural integrity, which included material and structural testing and modeling. This paper presents an overview of the entire research program and discusses the key results.

1. Introduction

Alkali aggregate reactions (AAR), particularly alkali-silica reaction (ASR), have been identified as occurring in the concrete of nuclear power plants (NPPs) in Canada and elsewhere. They have potentially serious implications on the structural integrity and/or serviceability of aging NPPs and there are no currently available assessment criteria or guidelines to assess the consequences. Therefore, an integrated study was conducted at the University of Toronto with funding support through a contract from the Canadian Nuclear Safety Commission. The work was focused on three aspects of this issue, namely: concrete materials, structural testing, and numerical analysis and assessment. By integrating the material and structural level studies and based on the numerical analysis, this study formulates key performance indicators and, in particular, structural assessment criteria for assessing nuclear concrete structures affected by ASR. Considering the large scope of the work, this paper mainly provides an overall view of the study and summarizes the key outcomes of the study. Citations are made to the related theses and research articles which can be referenced for an in-depth understanding of the study and its outcomes.

The materials aspects of the reaction have been extensively studied and most of the reaction mechanisms at the material level are understood. Many of the ASR studies and expansion measurements are based on unrestrained laboratory concrete specimens which limit the ability to predict multiaxial expansions in concrete structures, such as nuclear concrete structures, that are subjected to stresses or restraints in one or more directions. Key studies that have examined the effect of stress on the ASR expansion of concrete have primarily been uniaxial compressive stress (Kagimoto et al., 2014; Larive, 1998; Takahashi et al., 2015; Dunant and Scrivener, 2012). The primary outcome from these studies have been that expansion can be reduced in the stressed direction, and transferred to the unstressed directions. There is however a dearth of information on the relationship between ASR expansion and multi-axial stress state which forms the basis for the material level examination presented in this paper.

The materials part of this work is, therefore, focused on the characterization of ASR-affected concrete under multiaxial stresses. Some of the test measurements include: axial expansion, damage rating index (DRI) along three planes, nano-mechanical properties by nano-indentation; microstructural analysis; macro-mechanical properties by destructive and non-destructive tests; and evaluation of transport properties.

The structural part of the research program deals with the evaluation of the performance of squat shear walls made with ASR concrete

* Corresponding author.
E-mail address: d.panesar@utoronto.ca (D.K. Panesar).

https://doi.org/10.1016/j.nucengdes.2019.05.019
Received 16 November 2018; Received in revised form 15 May 2019; Accepted 17 May 2019
Available online 30 May 2019
0029-5493/

against similar squat shear walls made with normal concrete. Six shear walls were constructed, two with normal concrete and four with concrete containing reactive coarse aggregate. In addition, a large group of the control specimens consisting of twenty-one cylinders, three modulus of rupture beams, three expansion prisms, and three dog-bone specimens were cast for each type of the concrete. Fifty-two days after casting, the walls and control specimens were stored in an environmental chamber to accelerate the alkali-silica reaction. The temperature in the chamber was maintained at 50 °C and the relative humidity was 95%. All the walls were tested under reversed lateral cyclic displacement excursions while simultaneously subjected to constant axial load simulating seismic effects.

Two in-house non-linear finite element (FE) analysis programs, developed over the last two decades at the University of Toronto, VecTor2 and VecTor3 (VTAG, 2019), were adapted for the analysis of ASR-affected reinforced concrete structures. VecTor2 is applicable to concrete membrane structures, while VecTor3 is appropriate for the analysis of three-dimensional structures. The Modified Compression Field Theory (Vecchio and Collins, 1986) and the Disturbed Stress Field Model (Vecchio, 2000) form the theoretical basis of the programs. Reinforced concrete is treated as an orthotropic material based on a smeared rotating crack model within the context of a total-load secant-stiffness macro-modelling approach. The constitutive, compatibility, and equilibrium relationships are formulated in terms of average stresses and average strains (Vecchio 1990).

2. Materials level study

Two categories of specimens were prepared for this research, namely unrestrained and restrained specimens. The stress state of the cube specimens is shown in Table 1. Table 1 presents the seven different stress states considered in this study which include: 0, 3.9 MPa, and 9.6 MPa. The selected stress levels were chosen to be representative of typical prestressed nuclear concrete structures where Anderson (2005) reports 5–6 MPa stress and the vertical direction and 9–11 MPa in the horizontal direction based on field measurements from various containment structures in Sweden. The cube design details, construction approach and stress application methodology is detailed in Gautam and Panesar (2016). Table 1 presents seven stress states of the cube specimens, namely, no-stress (n), uniaxial (u or U), biaxial (b or B), and triaxial (t or T). Table 1 shows, the compressive stress value in the x, y, and z direction (namely, fx, fy, fz) for each of the stress states which defines its 'Designation'. Destructive and non-destructive tests were carried out at ages ranging from 28 days to 2 years.

The mix design was based on the concrete prism test as per ASTM C1293. The water-to-cement ratio was 0.44. High alkali general use (GU) cement was used with a total alkali content of 0.99% Na_2O equivalent by mass of cement. The alkali content of the mix was boosted to 1.25% Na_2O equivalent of cement by adding NaOH pellets to water prior to concrete mixing. Two types of concrete were considered, namely reactive and non-reactive (control). The reactive concrete was made with reactive coarse aggregate and non-reactive fine aggregate. The characterization of ASR affected concrete was based on Spratt aggregate as the reactive coarse aggregate, which is classified as a highly reactive aggregate (Thomas et al., 2012). The control concrete consisted of non-reactive fine and non-reactive coarse aggregates.

Table 1
Average applied compressive stress in concrete cube specimens for the seven stress states.

Stress state	Designation*	Average applied stress, MPa			Number of reactive cube specimens	Number of control cube specimens
		f_x	f_y	f_z		
No-stress (n)	n (0, 0, 0)	0	0	0	4	1
Uniaxial (u or U)	u (3.9, 0, 0)	3.9	0	0	3	1
	U (9.6, 0, 0)	9.6	0	0	3	1
Biaxial (b or B)	b (3.9, 3.9, 0)	3.9	3.9	0	3	1
	B (9.6, 3.9, 0)	9.6	3.9	0	3	1
Triaxial (t or T)	t (3.9, 3.9, 3.9)	3.9	3.9	3.9	3	1
	T (9.6, 3.9, 3.9)	9.6	3.9	3.9	3	1

Designation: stress state (fx, fy, fz).

The concrete was tested in two curing conditions employed to accelerate the ASR damage. (i) 38 °C temperature and relative humidity > 95%, which is typical of concrete prism test (CPT) and (ii) 50 °C temperature and > 95% relative humidity, considered in this study as accelerated concrete prism test (ACPT). The cube specimens were accelerated at 50 °C and > 95% relative humidity. Two sets of prisms and cylinders were investigated for the conditioning temperature of 50 °C and 38 °C.

Several tests were conducting on the prism specimens including: axial expansion, damage rating index (DRI), modulus of rupture, resonant frequency, ultrasonic pulse velocity (UPV) and surface resistivity. Cube specimens were measured for UPV and axial expansion along three directions. DRI was performed along three mutually perpendicular planes. Cores from the cube specimens were tested for static modulus of elasticity and compressive strength. Cylinders were tested for UPV, bulk resistivity, compressive strength and static modulus of elasticity.

3. Results and analysis from material study

This section presents few experimental results from the materials level study. The entire scope of the material level research has been disseminated in the PhD thesis of Gautam (2016). This body of work has been disseminated in a series of published journal papers which are briefly described. The sensitivity of the coarse aggregate grading was investigated (Gautam et al. 2017a) in order to evaluate the size effect of the aggregate on the extent and evolution of ASR damage in terms of expansion, mechanical properties. Panesar and Gautam (2016) have also investigated the mechanisms underlying the partial recovery of the mechanical properties of ASR affected concrete. Research on the development of the new method to apply long-term multiaxial stresses on concrete cube specimens is detailed in Gautam and Panesar (2016). The corresponding multiaxial stress- expansion relationship is presented and modeling in Gautam et al. (2017b). To understand the influence of elevated curing temperatures (38 °C vs > 50 °C), Gautam and Panesar (2017) conducted a comparative study to ensure that the ASR damage mechanism would not be altered with the elevated temperature, but only accelerated. This was significant in order to conduct the large number of tests in a reduced timeframe.

As detailed by Gautam and Panesar (Gautam and Panesar, 2017), an increase of 12 °C temperature from 38 to 50 °C, yields an expansion in ACPT to be 3.22 times faster than in CPT. Except for the rate of expansion, the general trend of expansion and the ultimate expansion were similar for both the ACPT and CPT specimens. These results indicate that despite having different rates, the trend and ultimate expansion are likely to be similar at different temperatures, and hence, ASR in concrete structures can be reasonably represented by experimental results from accelerated test methods.

Expansion is one of the most obvious effects of ASR and has been the fundamental indicator for ASR in concrete specimens. DRI appears as a suitable technique to indicate the performance of ASR-affected concrete. The modulus of rupture reduced by approximately 60% due to ASR. The splitting tensile strength was also highly sensitive to ASR. This is anticipated because ASR causes cracking, and tensile strength is directly influenced by cracking. Thus, structures that are critical to tensile strength are expected to be affected the worst by ASR. Modulus of elasticity for the non-reactive concrete increased by about 8% during one year of accelerated curing and it decreased by approximately 25% for the reactive concrete (Gautam et al., 2015). Compressive strength

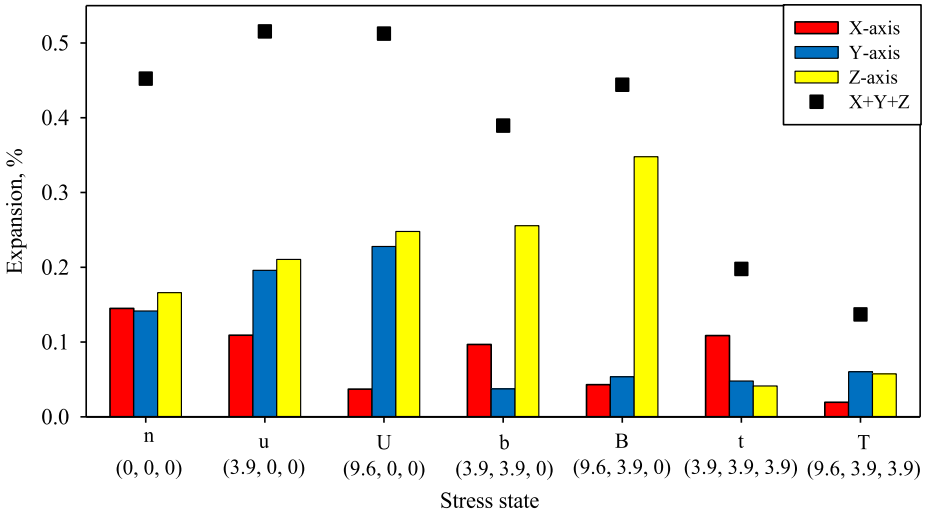

Fig. 1. Longitudinal and volumetric expansion (X + Y + Z) at 12 months of accelerated curing.

increased for both reactive and non-reactive concrete in the accelerated curing regime in this study and was not found sensitive to indicate the performance of concrete affected by ASR. Therefore, compressive strength of cores taken from an ASR-affected concrete structure may not be a suitable performance indicator for the structure unless compressive strength is the critical property.

The ultimate expansions for the various stress states are presented in Fig. 1. The standard deviations for all of the expansion measurements of the cube specimens at 360 days are low, and less than 0.053% (as shown in Table A1 in the ACI Materials journal paper (Gautam et al. (2017). Therefore, it is considered that the cube specimens can adequately reflect the intended tests. In addition, Gautam and Panesar (2016) have presented a discussion of the inter-specimen, intra-specimen and instrument variation of the specimens. Fig. 1 shows some marked differences in expansions among the different stress states. When the specimens were restrained biaxially in the X- and Y-directions, the expansion was suppressed in both of the stressed directions. Consequently, increased expansion was observed in the stress-free (Z) direction. The expansion in the Z-direction not only was significantly greater than the free expansion of the no-stress specimen, but also increased with an increased stress level in the X-direction. The volumetric expansion was significantly reduced for the triaxially stressed specimens. These results demonstrate a clear trend of expansion transfer from stressed to stress-free directions. The volumetric expansion due to ASR tries to get conserved as long as there is at least one unrestrained direction.

For concrete structures with restraint in one or two directions, expansion can be significantly suppressed in the restrained directions. However, significantly larger expansion can occur in the unrestrained directions. Based on the stress state in the other two perpendicular directions, the expansion in an unrestrained direction can be significantly greater than the unrestrained axial expansion, such as that indicated by the concrete prism test. For planar structures, such as walls, the out-of-plane expansion could be significantly larger than the in-plane expansion. Accordingly, monitoring the expansion in the stressed direction of a concrete element or structure may not be an adequate performance indicator as it can underestimate the extent of ASR damage on the structure.

DRI was sensitive to the stresses along different directions indicating that DRI in a concrete sample from a concrete structure should be performed along different planes to completely capture the extent of damage. Unlike the expansion measurement, DRI can be examined in a concrete sample without a previous reference measurement. Owing to the thorough examination capability of the concrete quality, increased sensitivity (compared to expansion), and insightful measurements even without a previous reference measurement, the DRI is recommended as an appropriate method to indicate the damage of an ASR-affected concrete structure.

Replicate cube specimens with all stress states were core drilled after unbolting at 3, 8 and 12 months of accelerated curing. The cores were tested for the modulus of elasticity and compressive strength. But, as previously indicated, the compressive strength does not well reflect the damage due to ASR. Therefore, Fig. 2 only presents the effect of stress direction on the static elastic modulus. The static elastic modulus was different between the two cores taken from stressed and unstressed directions of a pair of identical biaxially stressed specimens. These results indicated that ASR-affected concrete behaves orthotropically in the presence of different stresses along different directions.

The expansion results for various stress states were analyzed to develop an understanding on the effect of compressive stress on ASR expansion. The model was validated by analyzing the experimental cube specimens by using the finite element software VecTor3 (VTAG, 2019). Numerical results were in good agreement with the experimental results, thus validating the proposed model.

4. Structural level study

To evaluate the effects of varied ASR expansion over time on their structural performance, shear walls were tested in three phases, low

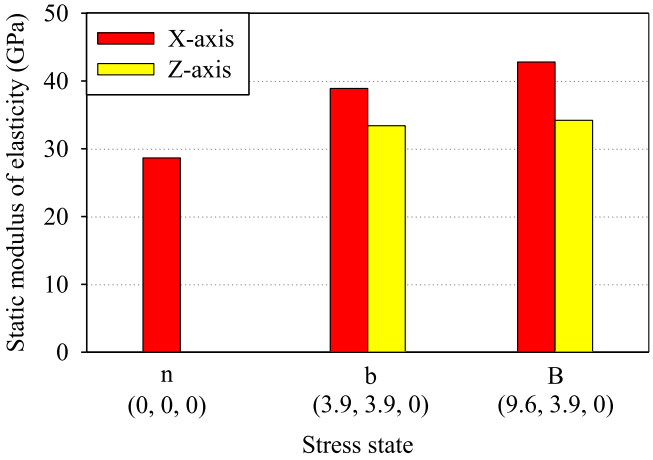

Fig. 2. Static modulus of elasticity along the stressed (X-axis) and unstressed (Z-axis) directions in the biaxially stressed specimens at 8 months of accelerated curing.

damage, moderate damage, and severe damage phase. 'Low damage phase' refers to a stage where the first ASR crack on the specimens can be detected by visual inspection. 'Moderate damage phase' refers to the time when patterns of ASR cracks are formed within the entire specimen. The 'severe damage phase' refers to the stage that the expansion due to ASR has reached its exhaustion level and no more expansion is expected from this point onward. Six prism specimens were cast for each type of concrete when the walls were constructed. These prisms were conditioned and monitored for expansion at 38 °C and 95% relative humidity. When the expansion reached a plateau, it was concluded that reaction has exhausted and severe damage phase is reached.

In this paper, results from two ASR shear walls A1 and B2 tested at low damage phase and severe damage phase, respectively, along with result from a regular shear wall REG B tested in phase 3 are presented. Based on the results from physical observations and monitoring of the specimens, first phase of structural testing was done around six months after conditioning of the specimens in the curing chamber commenced. The severe damage phase was reached after thirty-one months of storing the shear specimens in the environmental chamber.

All of the shear walls were identical in their geometry and reinforcement details. Fig. 3 shows the geometry of shear walls with elevation shown in Fig. 5a and the section of the walls shown in Fig. 5b. The beams and the boundary elements in the wall were designed with a high reinforcement ratio to ensure that no premature failure occurred in these elements before the failure of the internal wall panel occurred.

Testing of the shear walls employed two 1000 kN actuators and one hydraulic jack capable of applying and maintaining a constant 800 kN axial load. The shear wall was anchored to the strong floor and restrained from both sides to prevent any slippage. The force–displacement plot was obtained using the summation of the forces from both actuators against displacement of top of the shear panel (bottom of the top beam) with respect to the top of the lower beam. Further details of the structural testing and reinforcement details of the shear wall specimens are provided in Habibi et al. (2015).

5. Results and analysis from structural study

Table 2 presents a brief summary of the test results. The maximum capacity of the regular shear wall REG B was recorded as 1187 kN and the maximum capacity of the ASR shear walls, ASR A1 and ASR B2 was recorded as 1354.5 kN and 1242.7 kN, respectively.

As shown in Table 2, the ultimate shear capacity of these shear walls is approximately similar while a significant drop of maximum displacement and ductility is noticed between ASR A1 tested at 260 days and ASR B2 tested at 995 days. The REG B shear wall showed similar behavior, in terms of both ultimate lateral displacement and shear strength, in comparison with the ASR A1 wall which was tested at the low damage phase. However, comparing the REG B with ASR B2, both tested at the same age, noticeable performance degradation is observed. Lateral force vs. top deflection responses of the three shear walls are shown in Fig. 4.

Based on the results from the structural testing, in particular with comparison to the control specimens, it is believed that confinement played a critical role in determining the behavior of ASR A1 shear wall. In all three walls, the top and bottom beams, along with the two side boundary elements (columns), induced confinement in the specimens during testing. In the ASR specimens, this confinement was further enhanced due to the restraint developed as a result of expansion of concrete. Since the shear wall panel is restrained from all sides, the internal expansion of concrete due to ASR will add significantly to the confinement effect. Since expansion of ASR concrete occurs during curing and conditioning, the reinforcement in the shear wall will undergo a pre-stressing state thus resulting in a stiffer wall response compared with that of regular concrete wall. Therefore, at early stages of the damage, these two factors are most likely responsible for the increase in the ultimate strength and increased initial stiffness of the ASR specimen compared with the REG B and ASR B2 walls. The mode of failure is also accordingly affected by the state of confinement in both walls.

Three photos, 5a, 5b and 5c, in Fig. 5 show three walls REG B, ASR A1 and ASR B2, respectively at the end of tests. In the regular concrete specimen, the first cracks with widths less than about 0.4 mm appeared on the shear panel at displacement of about 1.2 mm. Cracks on the columns were initiated later in the test, at a displacement of about 3.5 mm. At 5 mm displacement, a huge crack was observed in the columns and at 6 mm displacement, spalling of concrete in column areas was observed. Within this cycle significant spalling of concrete on shear wall panel was noticed accompanied by a diagonal crack which became wider as displacement was increased. The wall carried the maximum load at about 7 mm deflection beyond which it showed a softening response while still maintaining the 800 kN applied axial load and lost its capacity at a displacement of about 8.1 mm. Final collapse of the specimen was due to sliding of the wall where it meets the bottom beam. Fig. 5 shows the regular shear wall at failure.

Both of the ASR shear wall specimens cracked initially at an early stage of the experiment, at a displacement of about 0.8 mm. Crack

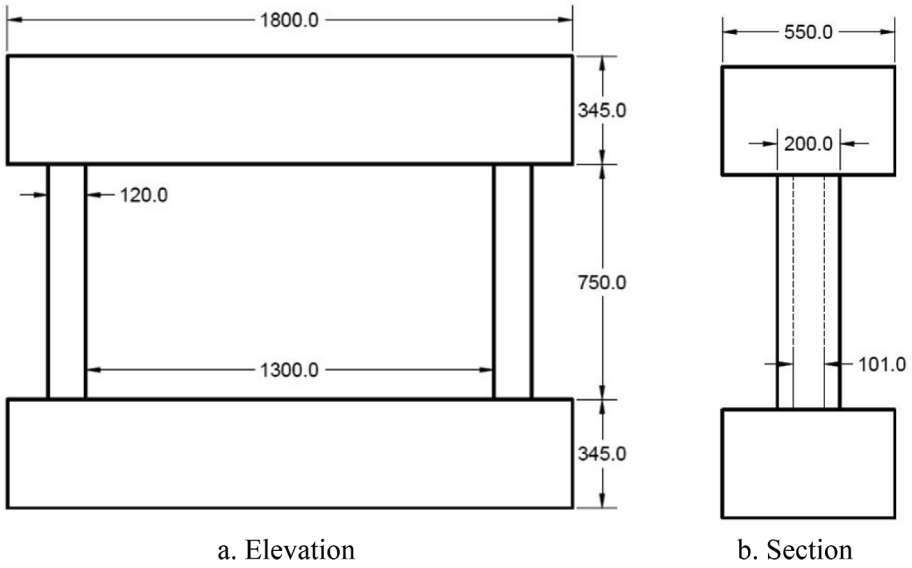

Fig. 3. Geometry of shear walls.

Table 2
Summary of results.

Wall	Age (days)	Compressive strength (MPa)	Expansion %	Peak force (kN)	Maximum displacement (mm)	Mode of failure
ASR A1	260	63.7	0.19	1354.5	7.1	Diagonal
ASR B2	995	63.0	0.223	1242.7	2.6	Diagonal
REG B	975	80.1	0.0331	1187	8.1	Sliding between the wall panel and the bottom beam

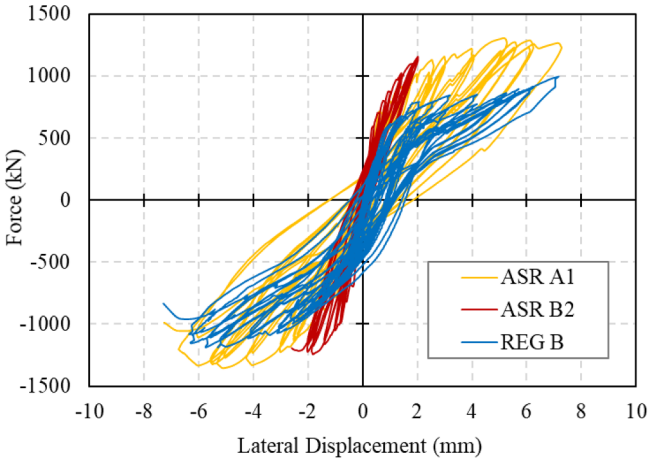

Fig. 4. Lateral load versus lateral displacement.

widths in this stage varied from 0.1 mm to 0.6 mm. More cracks then opened up, as displacement was increased. In the ASR A1 wall, at about 3 mm displacement, a notable diagonal crack was formed. No spalling of concrete was noticed on the shear wall. However, spalling of the concrete in the column area was observed at 6 mm displacement. At this stage the diagonal crack in the wall opened significantly and eventually the specimen failed to maintain the axial load when the lateral displacement was 7.1 mm. The specimen did not display any significant descending branch of the response. On the other hand, ASR B2 specimen showed noticeably more shear cracks at low displacement levels. These cracks widened as cycles progressed and eventually the wall failed at ultimate lateral displacement of 2.6 mm in a brittle manner. Fig. 5 presents the ASR shear walls at failure. The final collapse was due to shear failure in the wall panel.

6. Modeling and analysis

6.1. Modeling approach

The effect of ASR is simulated through two different mechanisms: the induced expansion, and the deterioration of mechanical properties. ASR expansion is treated as an elastic, non-recoverable offset strain, evaluated iteratively in the first load stage of the analysis. The procedure employed was previously developed for elastic and plastic offset strains (Vecchio, 1992). Average long-term loading conditions are considered when performing the ASR analysis. Six models were implemented for the evaluation of ASR-induced expansion: uniform in all directions, Charlwood, Curtis (personal communication, August 19, 2014), Saouma and Perotti (2006), Sellier et al. (2009), and Gautam et al. (2017b).

The magnitude of longitudinal expansion developed under stress-free conditions is a required parameter for the ASR analysis. It may be directly input by the user, or it may be evaluated using the Saouma and Perotti model or the Sellier model, both of which include a kinetics component. As such, provided that experimental data characterizing the reaction are available from laboratory tests, the free expansion may be determined. Two options are available for considering the changes in mechanical properties. One alternative consists of using the values of the material properties obtained from tests on cores sampled from the structure. The other option evaluates the compressive and tensile strengths, and the modulus of elasticity, as a function of the free expansion based on the ISE (1992) prescriptions. With the latter, lower bounds to the mechanical properties have been defined using values from tests performed on cubes, prisms and cylinders, and on cores extracted from structures. Both options disregard the directional nature of the degradation in mechanical properties caused by the stress level. Both approaches were implemented in the analysis programs.

The analyses presented in this paper were performed using the Gautam et al. (2017b) constitutive model for ASR. The model treats ASR expansion volumetrically and it calculates anisotropic expansion along the principal directions as a function of the stress state. The magnitude of longitudinal expansion developed under stress-free conditions as measured from ASTM C1293 prisms was used as an input for the ASR analysis.

Finite element analyses were performed to verify the analytical procedure and the ASR constitutive models implemented. The verification studies simulated the behavior of uniaxially loaded cylinders, middle-notched prisms tested under three-point loading, shear and flexural-critical reinforced and prestressed concrete beams, and shear walls.

The flexural-critical specimens investigated did not exhibit a significant reduction in either capacity or ductility due to ASR. Some shear-critical specimens, such as shear walls and reinforced concrete beams containing transverse reinforcement, showed an increase in strength caused by ASR; an opposite effect was observed in beams with no stirrups.

At the material level, with the exception of the model which

Fig. 5. Regular and ASR walls at failure.

evaluates ASR-induced expansion uniformly in all directions, the various available expansion models yielded similar results. As well, no significant difference in results was observed between the expansion models at the structural level.

The procedure showed reasonable accuracy in modeling the response of ASR-affected structures. For the twenty ASR-affected specimens analyzed, strengths with a mean calculated-to-experimental ratio of 0.93 and a coefficient of variation (COV) of 8.0% were obtained. The mean experimental-to-calculated ratio for the non-reactive control specimens was 0.97 with a COV of 11.8%. Details on the verification studies and the analytical procedure itself may be found in Ferche et al. (2017), Jurcut et al. (2015), and Jurcut (2015).

6.2. Finite element models of the shear walls

Finite element analyses were conducted to investigate the behavior of the shear walls tested at the University of Toronto. A mesh with a total of 4528 plane stress rectangular elements was used for modeling the shear wall specimens. The thicknesses of the elements were similar to those of the specimens' sections: the elements in the flanges had a thickness of 200 mm, the elements in the web had a thickness of 100 mm, while the elements in the top and bottom beams were 550 mm thick. All reinforcement was included in the concrete elements as smeared reinforcement.

The support condition was chosen such that it would be representative of the test set-up arrangement and not restrain the ASR expansion. Roller supports were defined along the bottom surface of the base, restraining the vertical degree-of-freedom. At the mid-depth of the bottom beam a roller support was defined with the degree-of-freedom restrained in the horizontal direction. The typical finite element model is shown in Fig. 6.

Three load cases were defined for the numerical analysis. Load Case I represented the vertical load applied at the mid-depth of the top beam as a nodal displacement. The point of application was chosen such that the rotation of the top beam is unrestrained, corresponding to the experimental set-up conditions. Load Case II consisted of the self-weight of the specimen applied as gravity loads to all the concrete elements. To account for the axial load of 800 kN, nodal forces were distributed along the upper face of the top beam as Load Case III. For the ASR-affected shear walls, the ASR-induced strains were analyzed with an iterative procedure in the first load stage of the analysis.

The concrete properties used for the FE analyses, as determined from 100 mm diameter cylinders on the day of test, are shown in Table 3. The concrete compressive strength, f'_c, and the modulus of elasticity, E_c, were the only concrete properties input, the rest were left as the default VecTor2 values. For the reactive specimens, the free expansions (ε_{ASR}), determined from expansion prisms, were input for the ASR analyses.

With the exception of the concrete compression model, the default

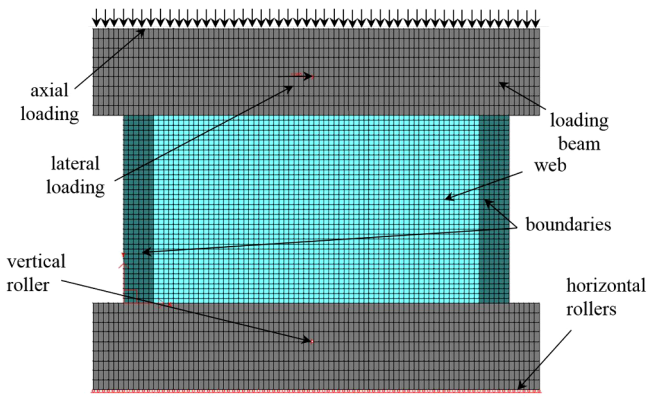

Fig. 6. Typical finite element model.

Table 3
Concrete properties.

Wall	f'_c (MPa)	E_c (MPa)	ε_{ASR} ($\times 10^{-3}$)
ASR A1	63.7	35,750	1.90
ASR B2	63.0	28,100	2.23
REG B	80.1	46,652	–

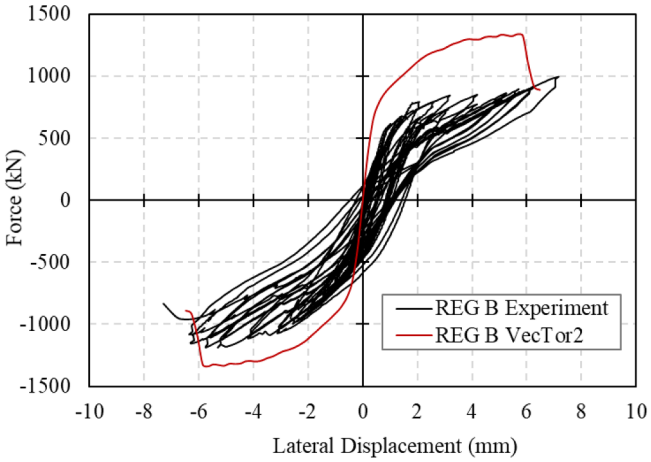

Fig. 7. Experiment versus FEA response for REG B wall.

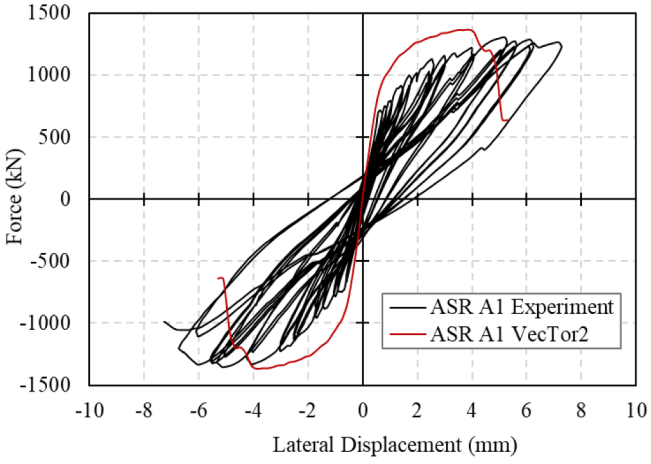

Fig. 8. Experiment versus FEA response for ASR A1 wall.

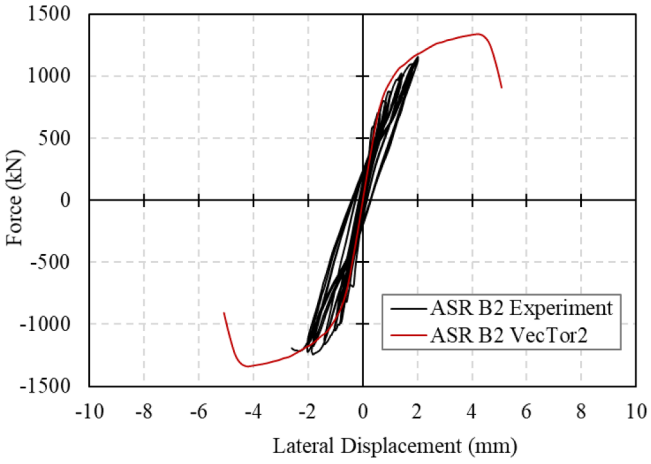

Fig. 9. Experiment versus FEA response for ASR B2 wall.

VecTor2 behavioral models for concrete and reinforcement were used. The Hoshikuma model for concrete in compression was selected for the analyses as it was found to be more suited to characterizing the behavior of high-strength concrete.

6.3. Experimental versus finite element analysis results

Several sensitivity studies were carried out in order to identify the mechanisms that play a significant role in the computed responses of the walls. The factors investigated were: mesh size, representation of boundary conditions, representation of the reinforcement, three-dimensional effects, strength enhancement due to confinement, bond strength, reinforcement buckling, cover spalling, concrete compression model, ASR strains calculations, and hysteretic response of concrete. Three factors were identified as having a notable effect on the computed response: the representation of boundary conditions, strength enhancement due to confinement, and concrete compression response. No significant strength degradation was observed analytically due to reverse cyclic loading; the monotonic pushover response was similar to the enveloped of the cyclic loading analysis. As such, to increase clarity in presenting the results, the monotonic behavior is compared with the experimental load-deflection plot. The comparisons between the analytical and experimental behaviors of walls, REG B, ASR A1 and ASR B2 are shown in Figs. 7–9.

For this type of specimens: shear-critical squat shear wall a large scatter in the numerical computed response is usually expected. A predictive approach was adopted for the analytical study, following a procedure characteristic for structural appraisal, with no effort to fine-tune the results to match the experimental observed behavior.

The computed behaviors for the reactive walls were also not significantly different, given the relatively similar concrete properties and the identical geometry and testing conditions; this outcome was expected. The experimentally measured responses of the reactive walls were significantly different however, with divergences that cannot be explained by differences in the measured concrete mechanical properties or expansion strains. The remaining shear wall specimens tested are currently being investigated, and the results will be presented in a future paper.

7. Concluding remarks

Key outcomes from this research on the materials aspects include: ASR expansion was suppressed due to stress and transferred to free or low stress directions; a constant volumetric expansion was observed for no-stress, uniaxial and biaxial; stress reduces the degradation of mechanical properties. Orientation of cracks was affected by stress such that the opening of cracks was in the direction of free or low stress.

Based on the results of the structural testing, it can be concluded that ASR did not affect the peak shear strength of the low aspect ratio shear walls. Confinement and pre-stressing of internal reinforcement due to ASR expansion resulted in higher initial stiffness and ultimate capacity of the ASR shear walls. However, ductility and ultimate lateral displacement of low aspect shear walls were considerably reduced as ASR expansion progressed.

Analytical studies have shown that the Disturbed Stress Field Model provides a viable platform for implementing ASR constitutive models into a nonlinear finite element analysis algorithm. Improved accuracy in computational methods could potentially be obtained provided that the following aspects are addressed in further studies:

1. Anisotropic expansion caused by multiaxial stress state is likely to cause non-uniform reductions in the concrete mechanical properties (ISE, 1992; Barbosa et al., 2018). This directionality aspect of the mechanical properties was not captured in the numerical work presented here, nor is it in other analyses reported in the literature.
2. Bond degradation between the reinforcement and concrete is expected to occur due to ASR-induced cracking. The development and implementation of a bond model suited for ASR-affected concrete is of particular interest for specimens where bond slip is a potential issue.
3. The influence of ASR on Poisson's ratio is currently not taken into consideration. An appropriate model will impact the level of confinement calculated.
4. The aggregate type is known to have an influence on the mechanical properties of reactive concrete (Giaccio et al., 2008). Constitutive models taking into account the particularities of different aggregate types should be developed and implemented.

References

Anderson, P., 2005. Thirty years of measured prestress at Swedish nuclear reactor containments. Nucl. Eng. Des. 235, 2323–2336. https://doi.org/10.1016/j.nucengdes.2005.04.002.

Barbosa, R.A., Hansen, S.G., Hansen, K.K., Hoang, L.C., 2018. Influence of alkali-silica reaction and crack orientation on the uniaxial compressive strength on concrete cores from slab bridges. Construct. Build. Mater. 176, 440–451.

Dunant, C.F., Scrivener, K.L., 2012. Effects of uniaxial stress on alkali-silica reaction induced expansion of concrete. Cem. Concr. Res. 42 (3), 567–576. https://doi.org/10.1016/j.cemconres.2011.12.004.

Ferche, A.C., Panesar, D.K., Sheikh, S.A., Vecchio, F.J., 2017. Toward macro-modeling of ASR-affected structures. ACI Struct. J. 114 (5), 1121–1129. https://doi.org/10.14359/51700778.

Gautam, B.P., 2016. Multiaxially Loaded Concrete Undergoing Alkali-Silica Reaction (ASR) (PhD thesis). University of Toronto, Toronto.

Gautam, B.P., Panesar, D.K., 2016. A new method of applying long-term multiaxial stresses in concrete specimens undergoing ASR, and their triaxial expansions. Mater. Struct. 49, 3495–3508. https://doi.org/10.1617/s11527-015-0734-z.

Gautam, B.P. , Panesar, D.K., Sheikh, S.A., Vecchio, F.J , Orbovic, N., 2015. Alkali aggregate reaction in nuclear concrete structures: Part2: concrete materials aspects. 23rd Conference on Structural Mechanics in Reactor Technology (SMiRT-23), Manchester, UK.

Gautam, B.P., Panesar, D.K., Sheikh, S.A., Vecchio, F.J., 2017a. Effect of coarse aggregate grading on the ASR expansion and damage of concrete. Cem. Concr. Res. 95, 75–83. https://doi.org/10.1016/j.cemconres.2017.02.022.

Gautam, B.P., Panesar, D.K., Sheikh, S.A., Vecchio, F.J., 2017b. Multiaxial expansion-stress relationship for alkali silica reaction-affected concrete. ACI Mater. J. 114, 171–184.

Gautam, B.P., Panesar, D.K., 2017. The effect of elevated conditioning temperature on the ASR expansion, cracking and properties of reactive Spratt aggregate concrete. Constr. Build. Mater. 140, 310–320. https://doi.org/10.1016/j.conbuildmat.2017.02.104.

Giaccio, G., Zerbino, R., Ponce, J.M., Batic, O.R., 2008. Mechanical behavior of concretes damaged by alkali-silica reaction. Cem. Concr. Res. 38 (7), 993–1004.

Habibi, F. et al., 2015. Alkali Aggregate Reaction in Nuclear Concrete Structures: Part 3: Structural Shear Wall Elements, SMiRT23, Manchester, U.K.

Institution of Structural Engineers (ISE), 1992. Structural Effects of Alkali-Silica Reaction. SETO, London.

Jurcut, A.C., 2015. Modelling of Alkali-Aggregate Reaction Effects in Reinforced Concrete Structures. MASc Thesis. , University of Toronto, pp. 136.

Jurcut, A. C., Vecchio, F. J., Sheikh, S. A., Panesar, D. K., and Orbovic, N., 2015. Alkali Aggregate Reaction in Nuclear Concrete Structures: Part 4: Modelling and Analysis. SMiRT23, Manchester, U. K.

Kagimoto, H., Yasuda, Y., Kawamura, M., 2014. ASR expansion, expansive pressure and cracking in concrete prisms under various degrees of restraint. Cem. Concr. Res. 59, 1–15. https://doi.org/10.1016/j.cemconres.2014.01.018.

Larive, C., 1998. Combined contribution of experiments and modelling to the understanding of alkali-aggregate reaction and its mechanical consequences. PhD thesis. Ecole Nationale des Ponts et Chausses, Marne-la-Vallée, France. (in French).

Panesar, D.K., Gautam B.P. 2016, The mechanisms behind the partial recovery in the degraded mechanical properties of ASR-affected concrete. Fib Symp., Cape Town, South Africa.

Saouma, V., Perotti, L., 2006. Constitutive model for alkali-aggregate reactions. ACI Mater. J. 103 (3), 194–202.

Sellier, A., Bourdarot, E., Multon, S., Cyr, M., Grimal, E., 2009. Combination of structural monitoring and laboratory tests for assessment of alkali-aggregate reaction swelling: application to gate structure dam. ACI Mater. J. 106 (3), 281–290.

Takahashi, Y., Shibata, K., Maruno, M., Maekawa, K., 2015. Uniaxial restraint tests under high-stress conditions and a chemo-hygral model for ASR expansion. Proceedings of the 10th International Conference on Mechanics and Physics of Creep, Shrinkage, and Durability of Concrete and Concrete Structures, Vienna, Austria, Sept., pp. 1061–1065.

Thomas, M.D.A., Folliard, K.J., Fournier, B., Ahlstrom, 2012. A prescriptive specification for the selection of measures for preventing alkali-silica reaction. 14th Int. Conf. Alkali Aggreg. Reaction, Texas.

Vecchio, F.J., 1990. Reinforced concrete membrane element formulations. J. Struct. Eng. 116 (3), 730–750.

Vecchio, F.J., 1992. Finite element modelling of concrete expansion and confinement. ASCE J. Struct. Eng. 118 (9), 46–56.

Vecchio, F.J., 2000. Disturbed stress field model for reinforced concrete: formulation. J. Struct. Eng. 126 (8), 1070–1077.

Vecchio, F.J., Collins, M.P., 1986. The modified compression field theory for reinforced concrete elements subjected to shear. ACI J. 83 (2), 219–231.

VTAG, 2019. VecTor2 and VecTor3: Nonlinear finite element analysis software for reinforced concrete structures. VecTor Analysis Group (VTAG), Retrieved from vectoranalysisgroup.com.